Precise Tailoring of Terahertz Short Pulse Semiconductor Sources with Gires–Tournois Interferometers and Active Mode-Locking

Valentino Pistore, Michael Schreiber, Anna De Vetter, Lukas Seitner, Hanond Nong, Juliette Mangeney, Jerome Tignon, Lianhe Li, Alexander Giles Davies, Edmund Harold Linfield, Christian Jirauschek, and Sukhdeep Dhillon**

V. Pistore
Laboratoire de Physique de l'Ecole Normale Supérieure, ENS, Université PSL, CNRS, Sorbonne Université, Université de Paris, 24 Rue Lhomond, 75005 Paris, France
Paul-Drude-Institut für Festkörperelektronik, Leibniz-Institut im Forschungsverbund Berlin e.V., Hausvogteiplatz 5-7, 10117 Berlin, Germany
E-mail: pistore@pdi-berlin.de

M. Schreiber, L. Seitner, C. Jirauschek
TUM School of Computation, Information and Technology, Technical University of Munich (TUM), Hans-Piloty-Str. 1, 85748 Garching bei München, Munich, Germany

A. De Vetter, H. Nong, J. Mangeney, J. Tignon, S. Dhillon
Laboratoire de Physique de l'Ecole Normale Supérieure, ENS, Université PSL, CNRS, Sorbonne Université, Université de Paris, 24 Rue Lhomond, 75005 Paris, France
E-mail: sukhdeep.dhillon@phys.ens.fr

L. Li, A. G. Davies, E. H. Linfield
School of Electronic and Electrical Engineering, University of Leeds, Woodhouse, Leeds LS2 9JT, United Kingdom

Funding: European Union's QuantERA II QATACOMB Project "Quantum correlations in terahertz QCL combs", the European Union's Horizon 2020 research and innovation Programme under grant agreement No 964735 (FET-OPEN EXTREME-IR).
EPSRC funding from the TeraCom project (Grant No. EP/W028921/1).

Keywords: Terahertz quantum cascade laser, Frequency comb, dispersion engineering, Gires-Tournois interferometer, active mode-locking, spectral tuning.

We present the complete control of the spectral and temporal emission properties of terahertz (THz) quantum cascade laser (QCL) pulsed frequency combs through engineered on-chip Gires–Tournois Interferometers (GTIs) and active mode-locking. By embedding GTIs directly into the laser waveguide, we tailor the chromatic dispersion profile to selectively enhance or suppress comb formation across the spectrum, using the precise dispersion of the GTI as a control parameter. This approach enables deterministic tuning of the comb's central frequency and bandwidth, allowing spectral shifts exceeding 300 GHz. Under active mode-locking, GTI-engineered devices produce near transform-limited pulses as short as 3.42 ps, even within narrow gain bandwidths. Time-domain simulations using a Maxwell–Bloch model confirm the experimentally observed spectral dynamics and provide insight into the underlying pulse formation mechanisms. We also report the emergence of strong spontaneous amplitude modulation in certain devices, which appears independent of external feedback and supports a natural pre-disposition toward pulse generation. Our results demonstrate that dispersion engineering via GTIs, in combination with active mode-locking, is a powerful and scalable technique for shaping THz QCL combs, offering precise control over their spectral and temporal characteristics. This enables new opportunities in high-resolution THz spectroscopy and dual-comb architectures with broadened spectral coverage.

1. Introduction

Terahertz (THz) quantum cascade lasers (QCLs) are compact semiconductor light sources that are based on intersubband transitions of electrons within a quantum well heterostructure.[1,2] They have demonstrated high output powers, exceeding 2 W in pulsed mode[3], and a broad frequency coverage spanning from 1.2 THz[4] to 6.0 THz.[5] THz QCLs have also exhibited ultra-narrow linewidths down to hundreds of Hz,[6] as well as spectrally broad frequency-comb (FC) operation enabled by intracavity four-wave mixing.[7,8] In recent years, active microwave/RF current modulation and injection techniques have further enabled coherent comb control,[9,10] harmonic comb states,[11] and actively mode-locked operation in THz QCLs.[12] Moreover, pulse-train generation with durations as short as 4 ps has been reported,[13] together with isolated pulses as short as 2.5 ps,[14] making them highly attractive for high-resolution spectroscopic applications, where frequency stability and coherence are essential.[15] A key advantage of THz QCLs is that their emission frequency is, a priori, determined by the design of the active region rather than by the material system, allowing precise spectral tailoring during the design process.[16]

Nonetheless, in the case of THz QCL FCs when in either frequency and amplitude modulated operation, once laser action is demonstrated, there is limited tunability of the spectrum profile, which is typically fixed by the spectral gain. This is problematic for applications such as heterodyne detection or gas-phase spectroscopy, where precise control of the central frequency would be extremely desirable to target particular spectral signatures.[17,18] Indeed for THz QCL FCs, tuning remains restricted to a few hundred MHz around the native emission band,[15] limiting their possible applications. On the other hand, FCs are inherently sensitive to dispersion. Optical feedback in combs, for example, can affect the dispersion by perturbing the carrier transport and gain saturation, which in turn modify both the emission frequency and the intermodal spacing.[19] This extreme sensitivity underscores the key role of dispersion in governing both the stability, and spectral and temporal characteristics of THz QCL FCs.[20–22]

In this work, we show how the broadband spectrum of actively mode-locked FC THz QCLs can be tuned deterministically across a significant portion of the gain bandwidth using only dispersion as the control element. Our approach involves a precisely engineered Gires–Tournois Interferometer (GTI) integrated with the QCL cavity[13] and exploiting the FC sensitivity to chromatic dispersion.[23] By applying a microwave modulation to the drive current of the laser (typically in the 5–20 GHz range here), we enforce active mode-locking[24,25] allowing to generate a FC where dispersion and gain conditions favor coherent pulse formation. The GTI introduces engineered dispersion into the cavity, and when combined with the active mode-locking, effectively locks the comb modes to a shifted spectral region of low dispersion. In addition to pulse generation down to 3.42 ps, we show the continuous control of central QCL frequency over at least 300 GHz using the active modulation frequency and over a doubling of the covered spectral region with engineered GTI compared to a standard QCL. To the best of our knowledge, no previously reported method offers comparable spectral flexibility in this frequency range and exceeds by a large margin what is achievable through conventional thermal or bias tuning.

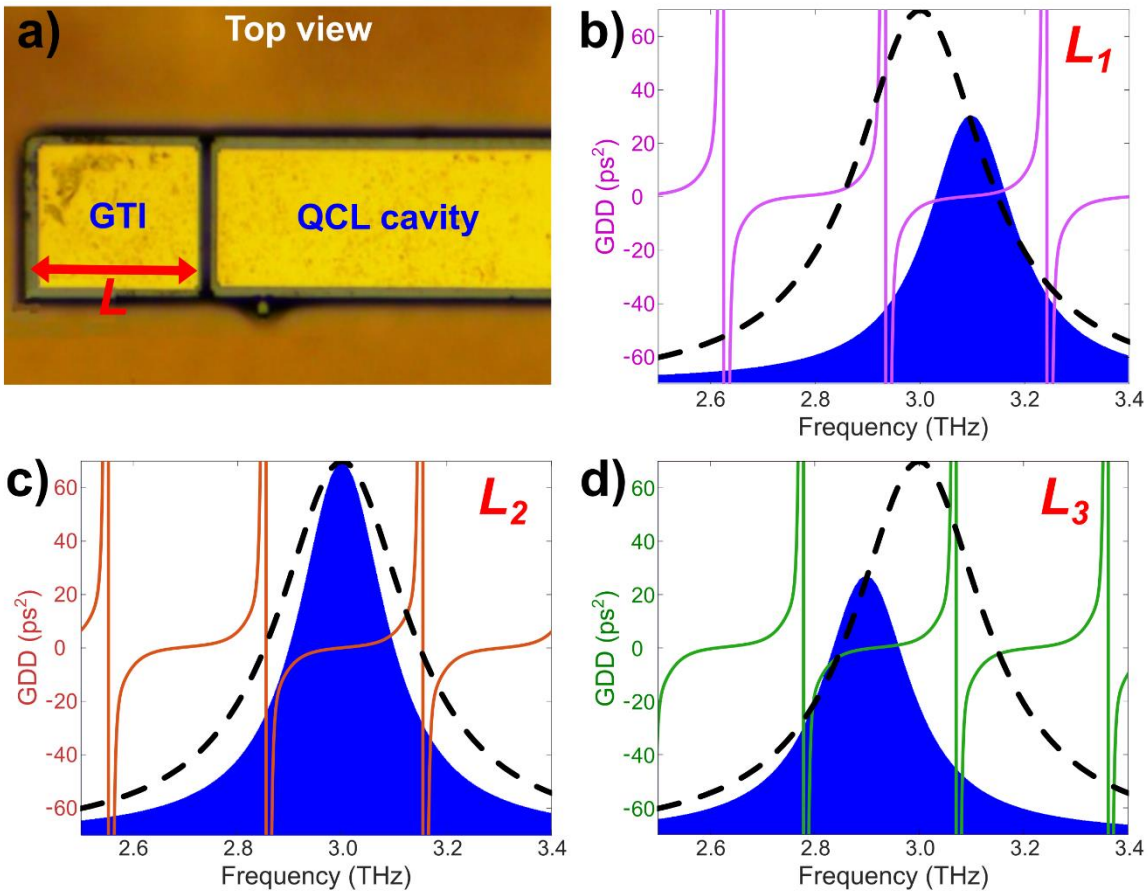


Figure 1: a. Top-view microscope image of one facet of a Fabry–Pérot THz QCL incorporating a Gires–Tournois Interferometer (GTI) of length L (total QCL length not shown). **b–d.** Schematic illustration of group delay dispersion (GDD) calculated using a 1D analytical model for increasing GTI lengths ($L_1 < L_2 < L_3$). The QCL gain spectrum is represented illustratively by a Lorentzian centered at 3 THz (black dashed curve) and the expected lasing bandwidth by the blue shaded area, conceptually depicting regions of low dispersion where mode-locking is favored.

The concept is illustrated schematically in **Figure 1**. Figure 1a presents a top-view microscope image of one end of a QCL cavity incorporating a GTI of length L. Figure 1b–d show representations of the corresponding group delay dispersion (GDD) calculated using an analytical 1D GTI model for increasing GTI lengths ($L_1 < L_2 < L_3$). The QCL gain is represented illustratively by a Lorentzian centered at 3 THz (black dashed curve). Under mode-locking conditions, the interplay between the GDD profile and the gain spectrum defines the frequency range in which lasing occurs (illustrated conceptually by the blue shaded regions in low-dispersion windows), enabling deterministic control of the emission frequency.

Beyond frequency tuning and spectral bandwidth control, our method enables the generation of stable trains of nearly transform-limited pulses by tailoring the GTI parameters to support coherent pulse formation. The experimental results are supported by comprehensive numerical simulations using a Maxwell–Bloch framework, which captures the interplay between chromatic dispersion, gain dynamics, and the active mode-locking mechanism. These simulations not only reproduce the observed spectral shifts but also reveal the underlying conditions that favor stable FC formation in the presence of engineered dispersion.

2. Results

We characterized the emission of the THz QCLs using an injection seeding technique and electro-optic detection within a terahertz time-domain spectroscopy (THz-TDS) system.[26] A comprehensive description of the measurement setup can be found in the Supporting Information (**Figure S1**). When a modulation at a frequency close to the cavity round-trip frequency (typically 5–20 GHz for 8–2 mm long resonators) is added on top of the QCL bias, the device exhibits significantly larger amplitude modulation through fixing of the mode spacing and phase, resulting in mode-locked pulse generation. In the frequency domain, this is associated with the emergence of additional longitudinal modes and a broadening of the emission bandwidth. However, under these conditions, the spectral changes, which include the shift of the central frequency, the broadening of the spectrum and the energy redistribution among the modes, are limited. This means that active mode-locking does not inherently provide a pathway towards controlling the spectral position of the comb in a deterministic manner.

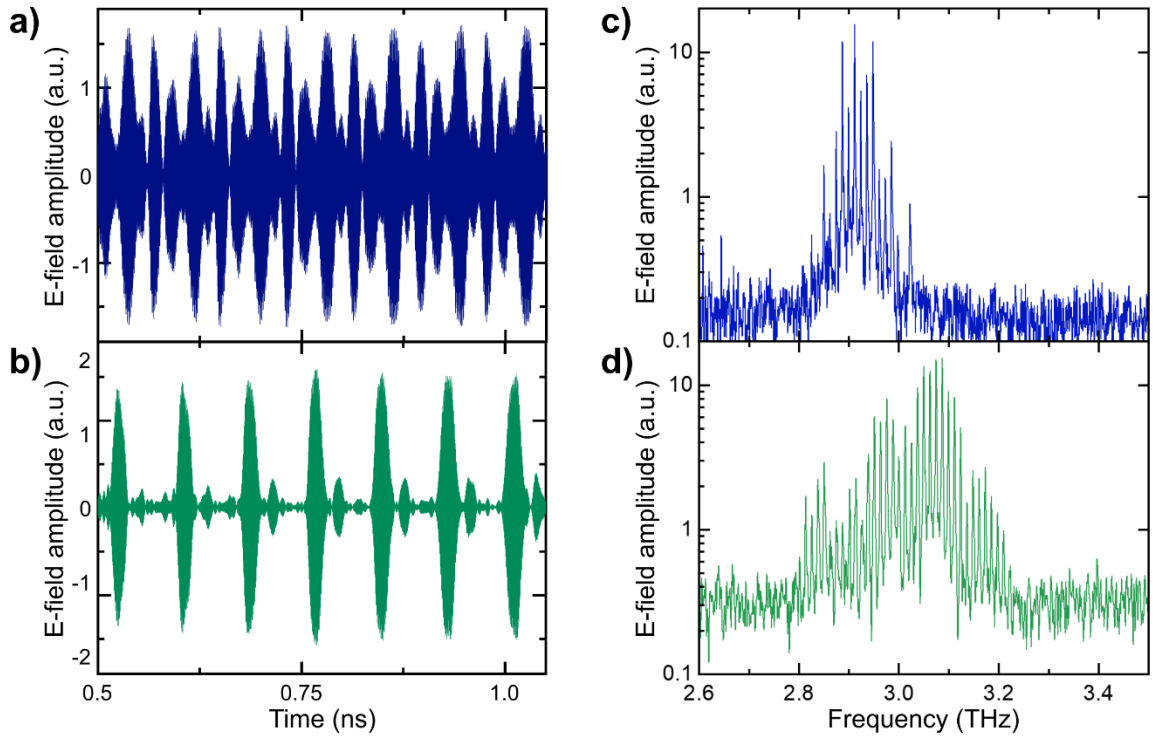


Figure 2: a-b. Experimental free-running emission (a) and mode-locking (modulation at 12.287 GHz) (b) time traces of FC_1. **c-d**. Fast Fourier Transform (FFT) spectra of the time traces in panels a-b.

In the experiments, the device under test consists of an active region composed of three gain modules centered at 2.5, 3.0, and 3.5 THz,[27] implemented in a double-metal waveguide geometry (3 mm × 56 µm × 15 µm) to ensure broadband operation and strong optical confinement. In the following, we shall refer to this device as FC_1. Its basic characterization, including the light-current-voltage characteristics and beatnote map, is reported in the Supporting Information (**Figure S2**). A clear distinction between the emission properties of a reference QCL (i.e., no GTI) without and with a round-trip active modulation at 12.3 GHz is illustrated in the time-domain traces shown in **Figure 2a** and **2b**, respectively, for a number of round-trips. The application of a Fast Fourier Transform (FFT) allows for the retrieval of the

corresponding spectral amplitudes (Figure 2c and 2d). As can be seen, when not mode-locked (Figure 2a), the emission profile does not show a clear pulse behavior with a limited number of spectral modes (Figure 2c - 2.85 THz – 3 THz). When mode-locked, we see a clear change with short pulse generation (Figure 2b) and an enlarged spectrum (Figure 2d - 2.8 – 3.2 THz). Note that, in this case, there appears to be no emission from the gain module at 3.5 THz.

Given the high sensitivity of THz QCL FCs to chromatic dispersion,[28] we exploit this as a means of tailoring the pulse and comb generation properties. To this end, we fabricated GTIs of varying lengths (36.1 µm, 37.1 µm, and 38.3 µm) at one end of the QCL waveguides on the same chip as FC_1, which is used as a reference. We shall refer to these devices with integrated GTIs as FC_1-#, with # being the length of the GTI. The GTIs were fabricated by introducing a ~ 2 µm gap in the active region using ICP etching, creating an embedded Fabry–Pérot coupled-cavity within the laser structure. The GDD profiles introduced by each GTI[13] were computed using full three-dimensional electromagnetic simulations in COMSOL Multiphysics, incorporating the exact geometrical features extracted from SEM pictures (**Figure S3**, Supporting Information). Details regarding the numerical methodology used to extract the GDD from the simulated complex S_{11} reflection coefficient are provided in the same section in the Supporting Information. The resulting dispersion curves are shown in **Figure 3a–c** (black lines). Notably, these simulated profiles deviate from the 1D theoretical model for GTIs,[13] highlighting the importance of accounting for the full 3D structure and fabrication-induced asymmetries when modeling GTI-induced dispersion profiles.

Each GTI was designed to exhibit a resonance, and thus strong dispersion, within the primary emission bandwidth of FC_1. The small (~ 1 µm) difference in the GTI lengths allows to study the sensitivity of the QCL's emission to small changes in the GTI designs. As the GTI length increases, the resonance shifts toward lower frequencies, effectively tuning the frequency of the strong dispersion region. This behavior is reflected in the corresponding mode-locked emission spectra (colored lines in Figure 3a–c), where gaps in the optical spectrum appear in regions of strong dispersion. These spectral gaps directly correspond to the resonance peaks in the calculated GDD profiles, confirming that high dispersion suppresses comb formation at those frequencies. A comparative overview is presented in Figure 3d, where the mode-locking spectra of the three QCLs with integrated GTIs are shown alongside FC_1. It is evident that as the GTI resonance shifts to lower frequencies, the emission band of the QCL shifts accordingly, avoiding regions of high dispersion. While large positive dispersion inhibits mode formation, moderate negative dispersion appears to favor mode-locking performance, likely by compensating for the material and gain component of the dispersion.[28] This leads to a more complex scenario than that in Figure 1, as the gain of FC_1 covers several hundreds of GHz and the dispersion profile of the 3D GTIs deviates from the 1D case. Furthermore, the spectral distribution of power on either side of the GTI resonance can be tuned by adjusting the GTI design parameters, providing a pathway not only for spectral shifting but also for shaping the laser emission profile. Conversely, this behaviour is not observed in the free-running case despite the dispersion (see Supporting Information, **Figure S4**), which shows that the spectral shifts are triggered by the combination of active mode-locking and strong GDD in the native emission band of the QCL. Interestingly, as well as re-shaping the spectral profile with the GTI in chosen spectral bands, we observe a doubling of the spectrum covered (2.74 THz – 3.54 THz)

compared to the reference GTI. This appears to be due to the gain module at 3.5 THz showing laser action as a result of lower dispersion at these frequencies. Specifically, as the GTI length is increased to 38.3 µm, the GDD resonance red-shifts deeper into the lower-frequency band. On its low-frequency side, the GTI contributes strong positive GDD that adds to the positive background material and waveguide dispersion. Under active mode-locking, this large net-positive dispersion introduces a severe phase-mismatch, increasing the threshold for pulse formation in that band. Through spatial and spectral gain competition within the active medium, power is preferentially directed into the upper-frequency spectral window (3.1–3.4 THz), where the negative GTI dispersion successfully compensates for the background dispersion, resulting in the complete suppression of the lower-frequency spectral lobe in FC_1-38.3.

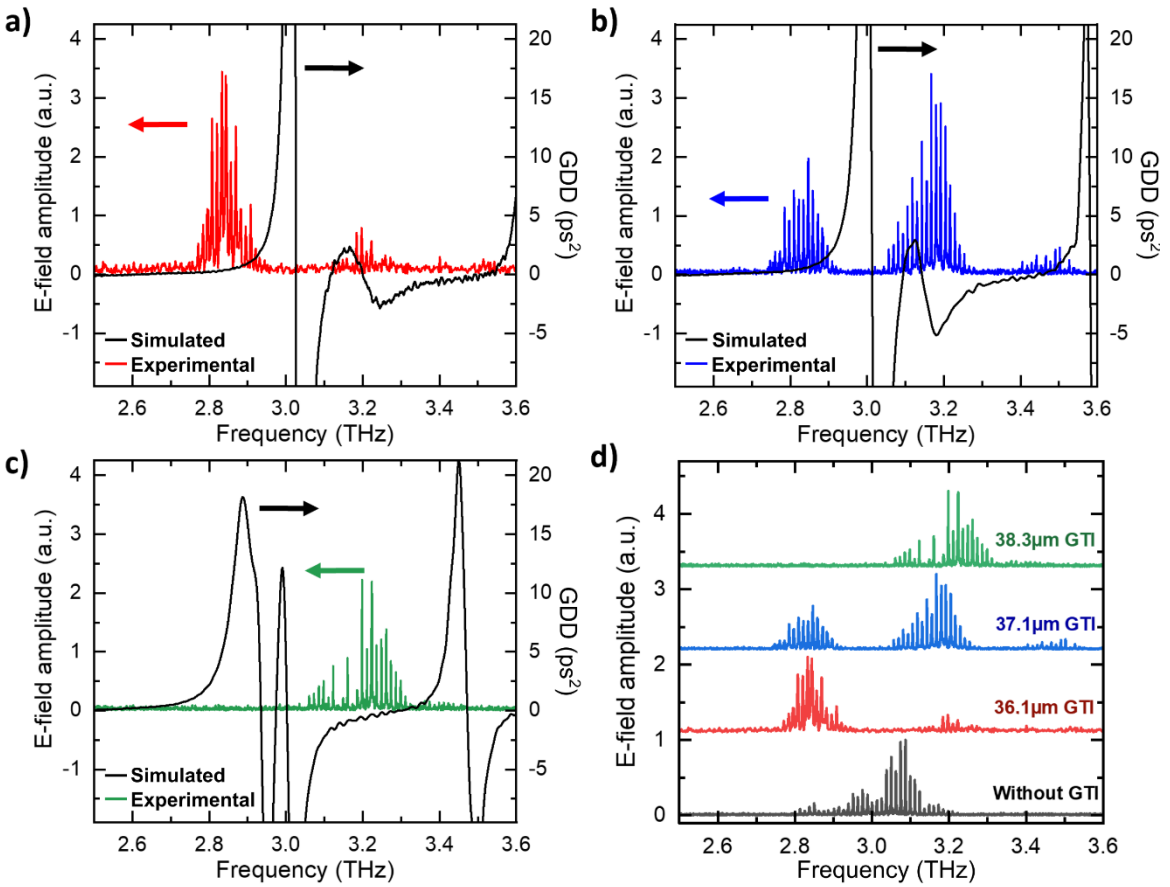


Figure 3: **a-c**. Experimental electric field spectral amplitude of the mode-locked emission of FC_1-36.1 (a, in red), FC_1-37.1 (b, in blue), and FC_1-38.3 (c, in green). The dispersion introduced by each GTI, computed from 3D COMSOL simulations based on the detailed SEM pictures of each individual structure (see Supporting Information, **Figure S3**), is plotted as the black solid curve in each panel. **d**. Comparison between the measured mode-locked normalized electric field amplitudes of FC_1 (reference) and the devices with the three different GTIs.

While the sensitivity of the frequency shifting mechanism to the GTI length was highlighted in the first set of devices discussed above, the following will show its dependence on the modulation frequency. As such, a second set of QCL devices from a second wafer growth, referred to as FC_2, was fabricated using the same active region design as the previous batch, and cleaved to a comparable length (~ 3 mm). One of the waveguides in this set was integrated with a 66.8 µm-long GTI at one end. **Figure 4a** shows the free-running (i.e., no active RF

modulation) electric field time traces of both FC_2 and FC_2-66.8. The respective spectra and optical intensity time-traces can be found in the Supporting Information, **Figure S5**. As a side note and beyond the scope of the current work, both devices exhibit strong spontaneous amplitude modulation in the time domain. While this behavior does not constitute self-mode-locking in the conventional sense, it likely reflects a coherent instability resulting from the interplay between active region design, cavity geometry, and chromatic dispersion. Crucially, however, the presence of this spontaneous modulation offers a favorable initial condition for active mode-locking, providing a natural tendency toward short-pulse formation, a feature that could be particularly advantageous for applications relying on high temporal resolution and high peak fields such as time-of-flight measurements and THz nonlinear optics. Conversely, for applications favoring constant-intensity emission, standard THz QCL fabrications typically yield frequency-modulated outputs (like FC_1) with limited spontaneous amplitude modulation.

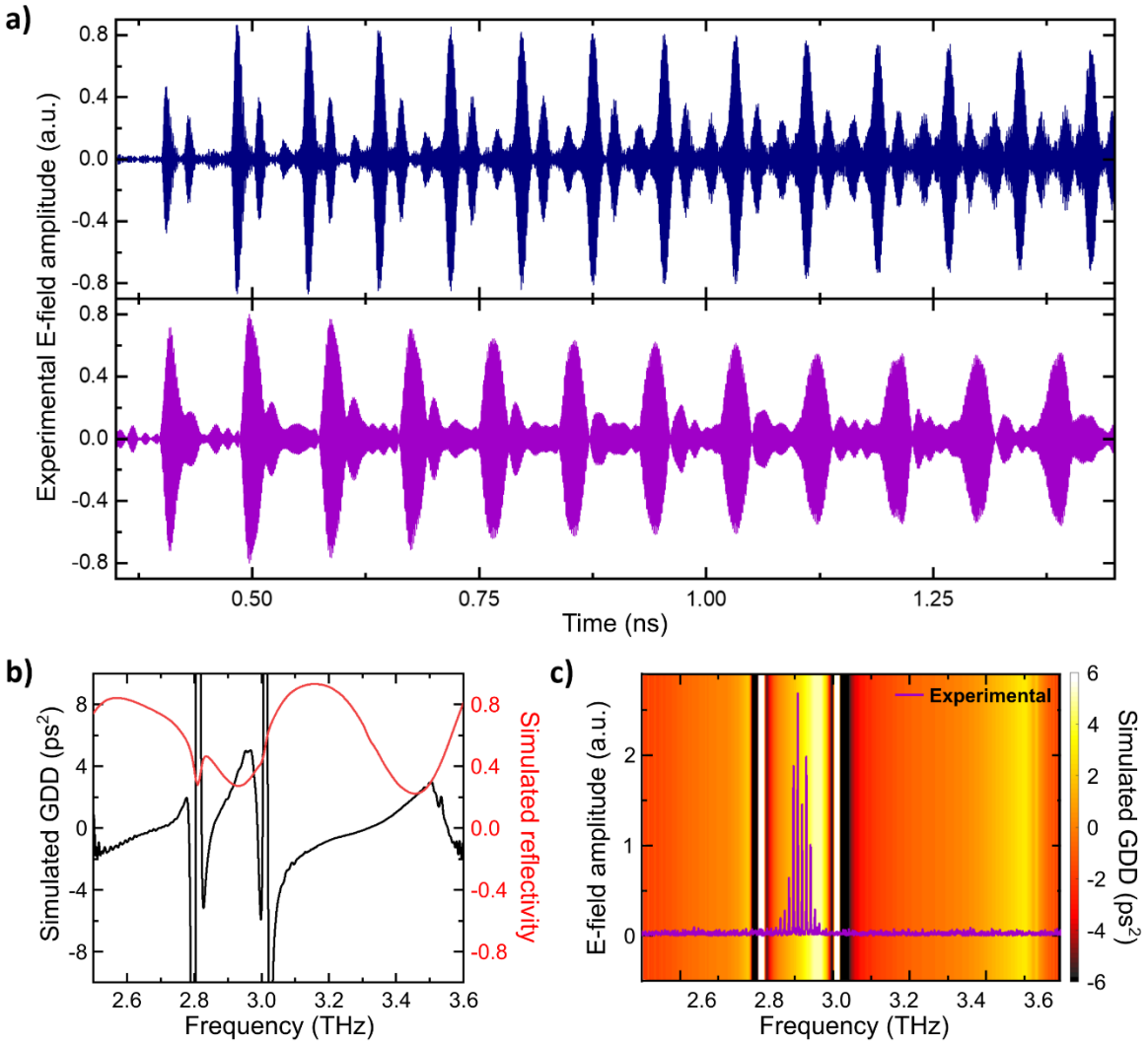


Figure 4: **a**. Experimental free running electric field emission of FC_2 (top, dark blue curve) and FC_2-66.8 (bottom, purple curve). **b**. Computed GDD and reflectivity of the integrated GTI obtained from 3D simulations on COMSOL Multiphysics. **c**. Experimental electric field spectral amplitude of the free-running FC_2-66.8. The introduced simulated GDD is displayed through a colormap and is the same as in (b).

This longer 66.8 µm-long GTI was specifically designed to introduce two distinct resonances at 2.8 THz and 3.0 THz, as shown in Figure 4b. These resonances impose a strong frequency-selective dispersion, effectively gating the free-running emission of the laser to the targeted spectral region (Figure 4c), with a mode spacing of ~ 11.26 GHz. Within this range, the dispersion is moderately positive, which translates in the time-domain electric field trace of FC_2-66.8 as relatively broad pulse-like features, in contrast to the sharper modulation observed in FC_2. In the absence of the GTI, FC_2 possesses a free-running spectrum centered around 2.95 THz (see Supplementary Information, **Figure S5**). This comparison suggests that when active mode-locking is applied to the device with the GTI, the emission spectrum is expected to shift toward higher frequencies where the dispersion is less.

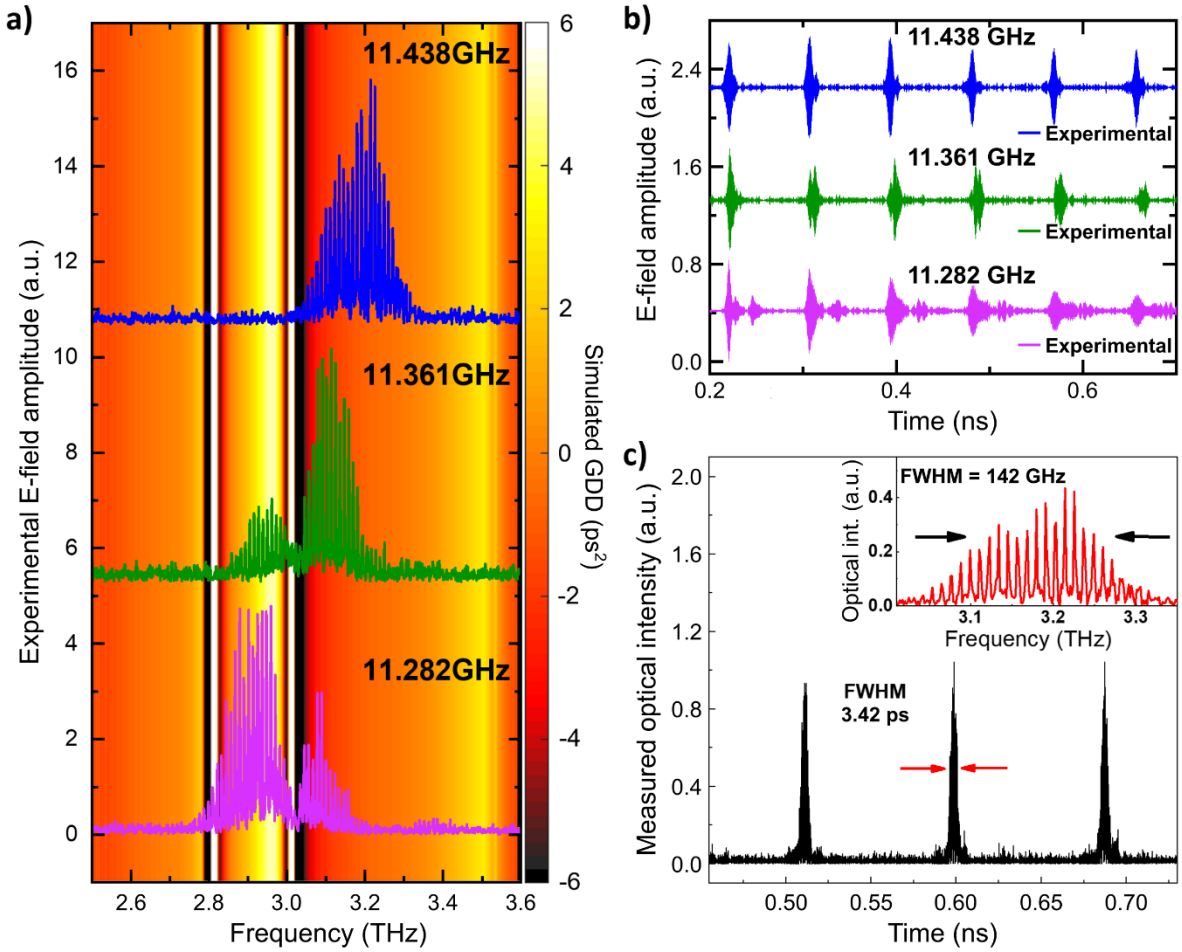


Figure 5: **a**. Experimental normalized electric field spectral amplitude of the mode-locked emission of FC_2 with a 66.8 µm long integrated GTI at different modulation frequencies. The background colormap represents the simulated dispersion introduced by the GTI. **b**. Measured electric field time traces corresponding to the spectra in (a). **c**. Experimental transform-limited 3.42 ps pulses obtained at 11.438 GHz mode-locking frequency. Inset: electric field spectrum of the associated time trace displaying a 142 GHz FWHM.

To validate our predictions regarding dispersion-induced spectral control, we applied active mode-locking to FC_2-66.8 using several modulation frequencies. The resulting emission spectra are presented in **Figure 5a**. When the modulation frequency is set to 11.282 GHz, relatively far from the cavity round-trip frequency, the spectrum exhibits two distinct lobes. One is confined below the GTI resonance, and a second portion appears above 3 THz. Notably, a pronounced

spectral hole remains at the resonance frequency, further confirming that strong positive dispersion inhibits mode formation and sideband generation in that region. As the modulation frequency is increased, first to 11.361 GHz and then to 11.438 GHz, closer to the actual round-trip frequency, the effectiveness of the active mode-locking improves significantly. This enhances coherent interaction among the cavity modes, enabling the spectrum to shift fully out of the high-dispersion region and extend entirely above 3 THz. This behavior confirms that the dispersion profile introduced by the GTI can not only be used to define the accessible spectral range but also to guide the spectral evolution under active mode-locking.

The corresponding electric field time traces for the three modulation cases are shown in Figure 5b. Only at the highest modulation frequency (11.438 GHz) does the laser exhibit a fully mode-locked regime, characterized by a clean, periodic, and highly stable train of THz pulses. Remarkably, the pulses generated under this condition exhibit a FWHM (derived from a Gaussian fit) of just 3.42 ps, despite the emission bandwidth being limited to a FWHM of 142 GHz (Figure 5c). This yields a time-bandwidth product of 0.485, which exceeds the theoretical Gaussian transform limit (0.441) by only 10%. This confirms that the pulses are nearly transform-limited, achieving the shortest possible duration allowed by their spectral width. Even more significantly, the emission band is shifted by over 300 GHz relative to the free-running spectrum, with no overlap between the original and mode-locked spectral ranges. One can compare with the active mode-locked emission of FC_2 in the Supporting Information, **Figure S6**, where no spectral shift is observed compared to the free-running case. These results are a clear demonstration of the effectiveness of the GTI-based dispersion engineering as a robust strategy to both spectrally shift and shorten THz pulses in QCL FCs under the active mode-locking regime.

We corroborate and generalize these findings through dynamical simulations of the device FC_2-66.8. To this end, we apply the Maxwell-Bloch equations[29,30] to model the spatio-temporal evolution of the optical cavity field interacting with a two-level quantum system, which mimics the active region dynamics of the QCL. By separating the longitudinal from the transversal field components, the model can be reduced to an effective 1D description, where all quantities only exhibit a dependence in the propagation direction z. Moreover, we invoke the rotating wave approximation (RWA) and the slowly varying envelope approximation (SVEA) to further reduce the numerical load of the simulations.[30] For the complex envelopes $E_{\pm}(z,t)$ of the optical field traveling in forward $(+)$ and backward directions $(-)$, this yields the propagation equation in the SVEA

$$v_{\mathrm{g}}^{-1}\,\partial_{\mathrm{t}}E_{\pm} \pm \partial_{\mathrm{z}}E_{\pm} = -\frac{\mathrm{i}}{2}\beta_2\,\partial_{\mathrm{t}}^2\,E_{\pm} - \frac{a}{2}\,E_{\pm} + \mathrm{i}p_{\pm}.$$

Here, v_{g} denotes the group velocity, β_2 the background group velocity dispersion, a the power loss coefficient, and $p_{\pm}$ the polarization. The latter can be directly computed from the Bloch equations, describing the evolution of the quantum system.[30] To obtain the needed parameters for the quantum system, carrier transport simulations based on the ensemble Monte-Carlo (EMC) method[31] are performed for the central active region.[32] Subsequently, two-level system parameters are fitted to match the gain dynamics of the obtained EMC results.[33]

We incorporate the co-propagation between the optical field and the injected microwave along the waveguide contacts,[34] by analytically solving the transmission line equations for the given Fabry-Perot cavity and taking the bias dependence of the Hamiltonian into account.[35]

Note that the GDD profile extracted from the 3D electromagnetic COMSOL simulations differs considerably from the theoretical 1D models for GTIs as mentioned above. Hence, here we develop an effective waveguide model for the device FC_2-66.8 to mimic the 3D dispersion curve within these 1D dynamical simulations. Here, the GTI is implemented by two short regions at the right end of the simulation domain, where their lengths are set to match the GDD profile extracted from the 3D simulations, allowing a direct comparison between modeled and experimental devices. In the dynamical simulations, the air slit of the GTI is modeled as a single-point reflector with a power reflectance of $R = 0.42$. We note that it is crucial for this approach to use phase corrected reflection coefficient in order to retrieve the correct dynamics of the laser with GTI.[36] A summary of the main parameters employed in the simulations is reported in Section 7 of the Supplementary Information.

Figure 6a–c shows the simulated electric field spectra of the FC_2-66.8 device under different modulation frequencies applied to the bias current (blue curves). The corresponding GDD profiles introduced by the simulated GTI are represented in red. The insets display the intermodal beatnotes resulting from the coherent beating of the simulated modes. Notably, in our simulations the GDD profiles resulting from the effective waveguide model are in good agreement with the dispersion curves derived from COMSOL and used in the experimental analysis. The spectral evolution observed in the simulations closely reproduces the behavior shown in the experimental results of **Figure 5a**. The primary difference lies in an offset in the modulation frequency required to achieve a similar spectral behavior, which is expected due to the difference in effective refractive index between the simulated and physical QCL cavities. Nevertheless, the qualitative agreement is excellent.

In all simulated cases, the emission band of the laser shifts out of the GTI's positive dispersion region, aligning with spectral regions where the GTI introduces a slightly negative GDD. This transition reproduces the experimentally observed blue-shift of the comb center frequency with increasing modulation frequency. Figure 6d–f presents the corresponding time-domain electric field traces and their instantaneous frequencies. The laser operates in a pulsed regime in all three cases, but the pulse duration is minimized when the optical spectrum is fully shifted into the negative dispersion regime (3.4 ps, Figure 6c and 6f). In the intermediate case (Figure 6b and 6e), where the spectrum exhibits a two-lobed structure, we observe a sharp beatnote accompanied by a non-periodic time-domain signal. This behavior can be attributed to the existence of two sub-combs,[37] which we identified by extracting the carrier envelope offset frequency f_{CEO}, clearly differing for both parts of the spectrum. The fast modulation of the pulse envelope visible in the time trace of Figure 6e appears to be associated with the frequency separation between the central peaks of the two spectral lobes. A similar beating effect can be observed, albeit less distinctly due to amplitude asymmetry between the two combs, in the middle trace of Figure 5b, which further confirms the strong correlation between the experimental and simulation results. Additionally, the instantaneous frequency extracted from the electric field phase shows a rapid temporal variation in the two-lobed case, distinctly faster than in the single-lobed ones. This behavior indicates strong temporal chirping and complex

pulse dynamics, likely due to the simultaneous excitation of two competing comb regimes within the cavity.

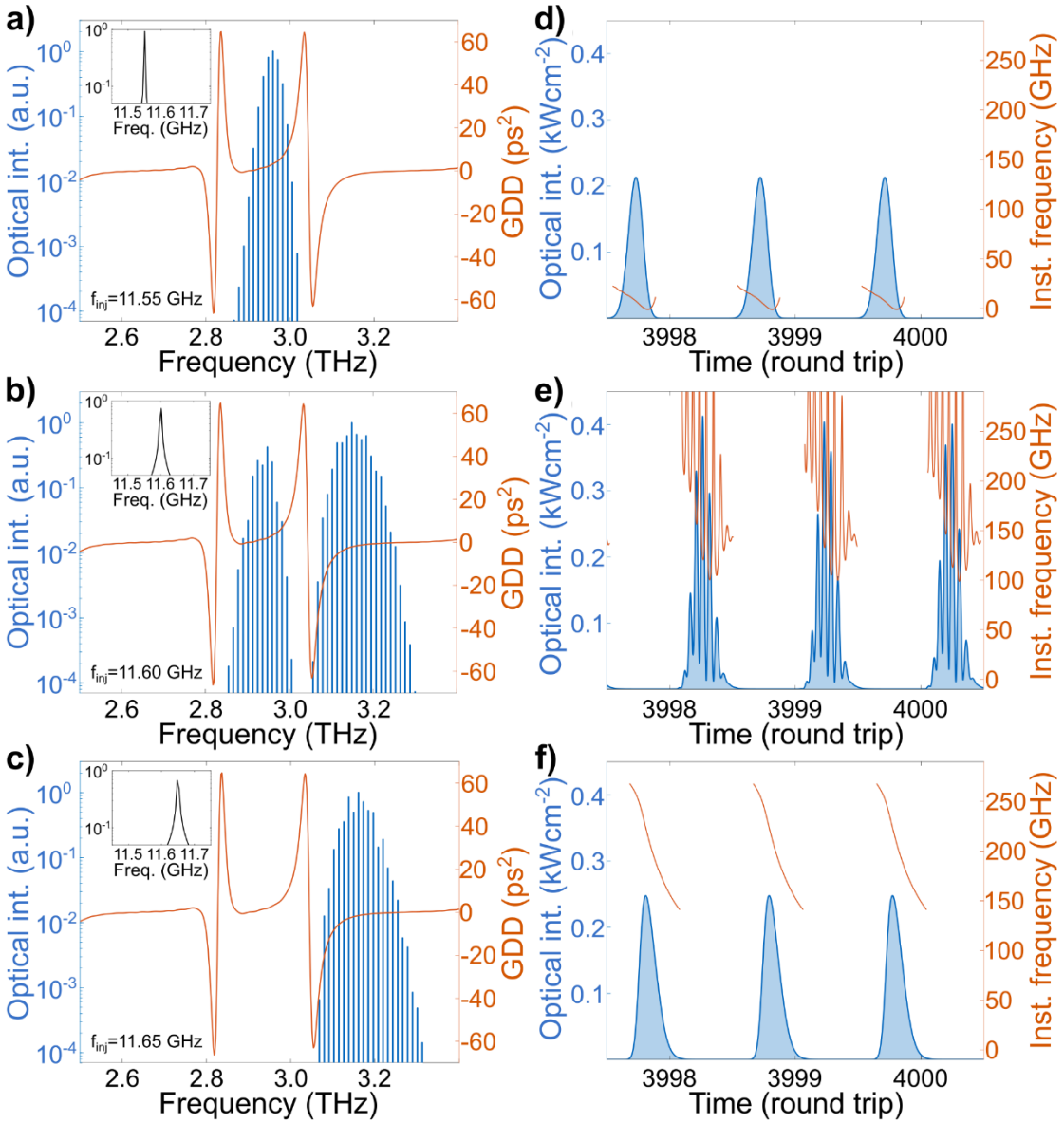


Figure 6: **a-c**. Simulated spectral intensity (blue curves) and GDD introduced by the GTI (red curves) of FC_2-66.8. Captions: simulated intermodal beatnotes. **d-f**. Simulated optical intensity time traces (blue curves) and instantaneous frequencies relative to the central frequency (red curves) of FC_2-66.8 associated with (a-c).

Some minor discrepancies between simulation and experiments arise in the spectral region between the GTI resonances, where positive dispersion is absent. Here, pulses exhibited comparable durations both when the spectrum was confined between the resonances and when it extended beyond them. As the dispersion landscape transitions from positive to negative, the leading and trailing pulse edges invert, yet no significant pulse length change is observed in the simulations (Figure 6d and 6f). This is most likely owing to the experimental positive dispersion being higher than that simulated, as a 1D model is used for these simulations.

Finally, simulation results using this formalism and illustrating the effect of different GTI lengths on the mode-locked spectra are reported in the Supplementary Information (**Figure S7**).

These results reproduce the spectral tuning arising from shifts in the GDD profile induced by varying the GTI length, in agreement with the experimental observations shown in Figure 3.

3. Discussion

In the absence of dispersion engineering via GTIs, the standard QCLs exhibited mode-locked behavior under appropriate RF modulation, but the resulting spectral features, namely the central frequency, bandwidth, and modal distribution, were not controllable or easily tunable (see Figure 2 and S5). The intrinsic sensitivity of QCL FCs to chromatic dispersion, long known to be a challenge,[28] was leveraged here as a degree of freedom. By embedding GTIs directly within the waveguide structure, we imposed custom, frequency-dependent dispersion profiles that allowed us to both suppress and enhance comb formation at specific spectral regions. The impact of this approach is two-fold. First, we demonstrated that regions of high positive dispersion introduced by GTI resonances inhibit the formation of comb modes. This suppression results in spectral gaps, effectively segmenting the emission spectrum and enabling spectral reshaping, as well as the controlled generation of multiple distinct combs within the same operating regime. Second, we showed that moderate negative dispersion not only permits but enhances mode-locking performance, facilitating shorter pulse durations. These effects were most pronounced in the FC_2-66.8 device, which featured two GTI resonances engineered to spectrally gate the emission around 2.8 and 3.0 THz. Upon applying mode-locking at a resonant modulation frequency, the emission band underwent a > 300 GHz blue-shift, and transform-limited pulses as short as 3.42 ps were generated, far shorter than what the unmodified device could produce.

Crucially, the experimental results were supported by time-domain simulations using a Maxwell–Bloch framework, where the GTI was modeled as a coupled resonant cavity. The simulations reproduced the spectral evolution observed in the experiments, including the two-lobed intermediate state and the complete spectral shift out of the positive GDD region. Furthermore, the simulations provided deeper insight into the time-domain dynamics, particularly the transient beating patterns and chirped pulses that emerge during spectral transitions. The strong agreement between experimental and simulated data underscores the robustness of the GTI approach and provides a foundation for predictive design of future dispersion profiles. The findings presented in our work open new pathways in the design of actively mode-locked THz QCLs. Unlike alternative approaches, GTI-based dispersion engineering offers a scalable and flexible solution, which is also easy to implement even on fully-fabricated devices using post-processing. Because the integrated GTI coupled-cavity is unbiased, short, and characterized by low optical losses within its predominantly GaAs-based waveguide, its dispersion mechanism is fundamentally passive and independent of the specific active region heterostructure. Consequently, this approach provides a highly transferable strategy using standard processing procedures for dispersion engineering across diverse THz QCL active regions and wafer designs. It enables precise control over the central frequency, bandwidth, and pulse duration, all of which are critical parameters for practical applications of THz FCs in spectroscopy, communications, and sensing.

4. Conclusion

In conclusion, we have experimentally demonstrated and theoretically validated an effective strategy to control the emission properties of pulsed THz QCL mode-locked and FC sources through integrated GTIs. By tailoring the GDD, GTIs enable selective suppression or enhancement of FC formation, allowing spectral shifts exceeding 300 GHz, as well as tunable and larger spectral bandwidths. Using this dispersion engineering approach, we achieved near transform-limited pulses as short as 3.42 ps, even within relatively narrow emission spectra. The strong agreement between experimental results and numerical time-domain simulations confirms both the robustness of our method and its potential for predictive device design. This establishes GTI-based dispersion engineering as a powerful tool for advancing the performance and flexibility of THz QCL FCs.

Beyond improving spectral and temporal coherence, our approach opens new pathways for application-specific tailoring. In particular, it could also offer significant potential for dual-comb spectroscopy, where QCLs incorporating GTIs of different lengths can access distinct spectral regions. This effectively extends the usable bandwidth and enhances the versatility of QCL-based systems for applications such as high-resolution spectroscopy.

Acknowledgements

The authors gratefully acknowledge Raffaele Colombelli and Souad Moumdji (Centre de Nanosciences et de Nanotechnologies, C2N) for fabricating the samples used in this work.

The authors acknowledge the support from the European Union's QuantERA II QATACOMB Project "Quantum correlations in terahertz QCL combs", the European Union's Horizon 2020 research and innovation Programme under grant agreement No 964735 (FET-OPEN EXTREME-IR). The authors also acknowledge EPSRC funding from the TeraCom project, Grant No. EP/W028921/1.

Data Availability Statement

The data that support the findings of this study are available from the corresponding authors upon reasonable request.

Received: ((will be filled in by the editorial staff))
Revised: ((will be filled in by the editorial staff))
Published online: ((will be filled in by the editorial staff))

References

[1] Faist, J., Capasso, F., Sivco, D. L., Sirtori, C., Hutchinson, A. L., Cho, A. Y., Quantum Cascade Laser, 1994, Science 264, 553, 10.1126/science.264.5158.553

[2] Köhler, R., Tredicucci, A., Beltram, F., Beere, H. E., Linfield, E. H., Davies, A. G., Ritchie, D. A., Iotti, R. C., Rossi, F., Terahertz Semiconductor-Heterostructure Laser, 2002, Nature 417, 156, 10.1038/417156a
[3] Li, L. H., Chen, L., Freeman, J. R., Salih, M., Dean, P., Davies, A. G., Linfield, E. H., Multi-Watt high-power THz frequency quantum cascade lasers, 2017, Electronics Letters 53, 799, 10.1049/el.2017.0662
[4] Walther, C., Fischer, M., Scalari, G., Terazzi, R., Hoyler, N., Faist, J., Quantum cascade lasers operating from 1.2 to 1.6 THz, 2007, Applied Physics Letters 91, 131122, 10.1063/1.2793177
[5] Shahili, M., Addamane, S. J., Kim, A. D., Curwen, C. A., Kawamura, J. H., Williams, B. S., Continuous-wave GaAs/AlGaAs quantum cascade laser at 5.7 THz, 2024, Nanophotonics 13, 1735, 10.1515/nanoph-2023-0726
[6] Vitiello, M. S., Consolino, L., Bartalini, S., Taschin, A., Tredicucci, A., Inguscio, M., De Natale, P., Quantum-limited frequency fluctuations in a terahertz laser, 2012, Nature Photonics 6, 525, 10.1038/nphoton.2012.145
[7] Burghoff, D., Kao, T.-Y., Han, N., Chan, C. W. I., Cai, X., Yang, Y., Hayton, D. J., Gao, J.-R., Reno, J. L., Hu, Q., Terahertz laser frequency combs, 2014, Nature Photonics 8, 462, 10.1038/nphoton.2014.85
[8] Faist, J., Villares, G., Scalari, G., Rösch, M., Bonzon, C., Hugi, A., Beck, M., Quantum Cascade Laser Frequency Combs, 2016, Nanophotonics 5, 272, 10.1515/nanoph-2016-0015
[9] Forrer, A., Franckié, M., Stark, D., Olariu, T., Beck, M., Faist, J., Scalari, G., Photon-driven broadband emission and frequency comb RF injection locking in THz quantum cascade lasers, 2020, ACS Photonics 7, 784, 10.1021/acsphotonics.9b01629
[10] Senica, U., Schreiber, M. A., Raffa, M., Micheletti, P., Beck, M., Jirauschek, C., Faist, J., Scalari, G., 2026, Nature 652, 892, 10.1038/s41586-026-10387-w
[11] Wang, F., Pistore, V., Riesch, M., Nong, H., Vigneron, P.-B., Colombelli, R., Parillaud, O., Mangeney, J., Tignon, J., Jirauschek, C., Dhillon, S. S., Ultrafast response of harmonic modelocked THz lasers, 2020, Light Sci Appl 9, 51, 10.1038/s41377-020-0288-x
[12] Senica, U., Forrer, A., Olariu, T., Micheletti, P., Cibella, S., Torrioli, G., Beck, M., Faist, J., Scalari, G., Planarized THz quantum cascade lasers for broadband coherent photonics, 2022, Light Sci Appl 11, 347, 10.1038/s41377-022-01058-2
[13] Wang, F., Nong, H., Fobbe, T., Pistore, V., Houver, S., Markmann, S., Jukam, N., et al., Short Terahertz Pulse Generation from a Dispersion Compensated Modelocked Semiconductor Laser, 2017, Laser & Photonics Reviews 11, 1700013, 10.1002/lpor.201700013
[14] Bachmann, D., Rösch, M., Süess, M. J., Beck, M., Unterrainer, K., Darmo, J., Faist, J., Scalari, G., Short pulse generation and mode control of broadband terahertz quantum cascade lasers, 2016, Optica 3, 1087, 10.1364/OPTICA.3.001087
[15] Bartalini, S., Consolino, L., Cancio, P., De Natale, P., Bartolini, P. Taschin, A., De Pas, M., et al., Frequency-Comb-Assisted Terahertz Quantum Cascade Laser Spectroscopy, 2014, Phys. Rev. X 4, 021006, 10.1103/PhysRevX.4.021006
[16] B. S. Williams, Terahertz quantum-cascade lasers, 2007, Nature Photonics 1, 517, 10.1038/nphoton.2007.166
[17] Lü, X., Röben, B., Pistore, V., Biermann, K., Luna, E., Wienold, M., Hübers, H.-W., et al., Terahertz quantum-cascade lasers: From design to applications, 2024, IEEE Transactions on Terahertz Science and Technology 14, 579, 10.1109/TTHZ.2024.3415501
[18] Gao, L., Feng, C., Zhao, X., Recent developments in terahertz quantum cascade lasers for practical applications, 2023, Nanotechnology Reviews 12, 20230115, 10.1515/ntrev-2023-0115

[19] Pistore, V., Pogna, E. A. A., Viti, L., Li, L., Davies, A. G., Linfield, E. H., Vitiello, M. S., Self-Induced Phase Locking of Terahertz Frequency Combs in a Phase-Sensitive Hyperspectral Near-Field Nanoscope, 2022, Advanced Science 9, 2270181, 10.1002/advs.202270181
[20] F. P. Mezzapesa, V. Pistore, K. Garrasi, L. Li, A. G. Davies, E. H. Linfield, S. Dhillon, M. S. Vitiello, Tunable and compact dispersion compensation of broadband THz quantum cascade laser frequency combs, 2019, Opt. Express 27, 20231, 10.1364/OE.27.020231
[21] Mezzapesa, F. P., Garrasi, K., Schmidt, J., Salemi, L., Pistore, V., Li, L., Davies, A. G., Linfield, E. H., Riesch, M., Jirauschek, C., Carey, T., Torrisi, F., Ferrari, A. C., Vitiello, M. S., Terahertz Frequency Combs Exploiting an On-Chip, Solution-Processed, Graphene-Quantum Cascade Laser Coupled-Cavity, 2020, ACS Photonics 7, 3489, 10.1021/acsphotonics.0c01523
[22] Mezzapesa, F. P., Viti, L., Li, L., Pistore, V., Dhillon, S., Davies, A. G., Linfield, E. H., Vitiello, M. S., Chip-Scale Terahertz Frequency Combs through Integrated Intersubband Polariton Bleaching, 2021, Laser & Photonics Reviews 15, 2000575, 10.1002/lpor.202000575
[23] Villares, G., Riedi, S., Wolf, J., Kazakov, D., Süess, M. J., Jouy, P., Beck, M., et al., Dispersion engineering of quantum cascade laser frequency combs, 2016, Optica 3, 252, 10.1364/OPTICA.3.000252
[24] Barbieri, S., Ravaro, M., Gellie, P., Santarelli, G., Manquest, C., Sirtori, C., Khanna, S. P., et al., Coherent sampling of active mode-locked terahertz quantum cascade lasers and frequency synthesis, 2011, Nature Photonics 5, 306, 10.1038/nphoton.2011.49
[25] Freeman, J. R., Maysonnave, J., Jukam, N., Cavalié, P., Maussang, K., Beere, H. E., Ritchie, D. A., et al., Direct intensity sampling of a modelocked terahertz quantum cascade laser, 2012, Applied Physics Letters 101, 181115, 10.1063/1.4765660
[26] Oustinov, D., Jukam, N., Rungsawang, R., Madéo, J., Barbieri, S., Filloux, P., et al., Phase seeding of a terahertz quantum cascade laser, 2010, Nature Communicaions 1, 69, 10.1038/ncomms1068
[27] Wienold, M., Schrottke, L., Giehler, M., Hey, R., Anders, W., Grahn, H. T., Low-voltage terahertz quantum-cascade lasers based on LO-phonon-assisted interminiband transitions, 2009, Electronics Letters 45, 1030, 10.1049/el.2009.1371
[28] Burghoff, D., Yang, Y., Reno, J. L., Hu, Q., Dispersion dynamics of quantum cascade lasers, 2016, Optica 3, 1362, 10.1364/OPTICA.3.001362
[29] Allen, L., Eberly, J. H., 1987, Optical Resonance and Two-Level Atoms, Courier Corporation, ISBN: 0486655334
[30] Jirauschek, C., Riesch, M., Tzenov, P., Optoelectronic Device Simulations Based on Macroscopic Maxwell–Bloch Equations, 2019, Advanced Theory and Simulations 2, 1900018, 10.1002/adts.201900018
[31] Jirauschek, C., Kubis, T., Modeling techniques for quantum cascade lasers, 2014, Applied Physics Reviews 1, 011307, 10.1063/1.4863665
[32] Riccardi, E., Pistore, V., Kang, S.-R. D., Seitner, L., Vetter, A. D., Jirauschek, C., Mangeney, J., et al., Short pulse generation from a graphene-coupled passively mode-locked terahertz laser, 2023, Nature Photonics volume 17, 607–614, 10.1038/s41566-023-01195-z
[33] Seitner, L., Popp, J., Haider, M., Dhillon, S. S., Vitiello, M. S., Jirauschek, C., Theoretical model of passive mode-locking in terahertz quantum cascade lasers with distributed saturable absorbers, 2024, Nanophotonics 13, 1823, 10.1515/nanoph-2023-0657
[34] Jirauschek, C., Theory of Hybrid Microwave–Photonic Quantum Devices, 2023, Laser & Photonics Reviews 17, 2300461, 10.1002/lpor.202300461
[35] Schreiber, M. A., Senica, U., Stowasser, J., Seitner, L., Haider, M., Scalari, G., Jirauschek, C., Dynamic modeling of mode-locked pulses and frequency combs in strongly

microwave-modulated semiconductor lasers, 2025, APL Photonics 10, 116107, 10.1063/5.0270594
[36] Seitner, L., Schreiber, M. A., Rinderle, M., Pichel, N., Haider, M., and Jirauschek, C., Aspects of cavity engineering in THz quantum cascade laser frequency combs, 2025, Nanophotonics 14, 3469-3482, 10.1515/nanoph-2025-0145
[37] Li, H., Laffaille, P., Gacemi, D., Apfel, M., Sirtori, C., Leonardon, J., Santarelli, G., et al., Dynamics of ultra-broadband terahertz quantum cascade lasers for comb operation, 2015, Opt. Express 23, 33270-33294, 10.1364/OE.23.033270

Supporting Information

Supporting Information is available from the Wiley Online Library or from the author.